RESEARCH PAPER

Interface creep behavior of grouted anchors in clayey soils: effect of soil moisture condition

Genbao Zhang[3] · Changfu Chen[1,2] · Jorge G. Zornberg[4] · Amr M. Morsy[5] · Fengshan Mao[1,2]

Abstract

This study aims at investigating the influence of moisture conditions on interface shear behavior of element-grouted anchor specimens embedded in clayey soils. The tests involved comparatively short embedment lengths and a device that was specially designed to facilitate moisture conditioning. Rapidly loaded pullout tests as well as pullout tests under sustained (creep) loading were conducted to characterize both the short-term and long-term ultimate shear strength of anchor–soil interfaces. Both values of the interface shear strength were found to decrease exponentially with increasing moisture content values, although their ratio was found to show a linearly decreasing trend with increasing moisture content. The interface shear creep response under pullout conditions was characterized by a rheological hybrid model that could be calibrated using experimental measurements obtained under increasing stress levels. The accuracy of the hybrid model was examined by evaluating the stress-dependent prediction model as well as its governing parameters. This investigation uncovers the coupled impact of soil moisture condition and external stress state on the time-dependent performance of grouted anchors embedded in clayey soils by correlating the interface shear strength with soil moisture content and associating the creep model with stress levels applied to the grout–soil interface.

Keywords Anchor–soil interface · Hybrid rheological model · Interface creep · Pullout test · Shear strength

1 Introduction

Anchorage techniques were initially used to strengthen the structural integrity of masonry dams and were then increasingly adopted to stabilize earth slopes and excavations into various soil types, including clayey soils [16, 53].

✉ Changfu Chen
cfchen@hnu.edu.cn

1 Key Laboratory of Building Safety and Energy Efficiency of Ministry of Education, Hunan University, Changsha 410082, Hunan, People's Republic of China

2 College of Civil Engineering, Hunan University, Changsha 410082, Hunan, People's Republic of China

3 College of Civil Engineering, Hunan City University, Yiyang 413000, Hunan, People's Republic of China

4 Department of Civil, Architecture and Environmental Engineering, The University of Texas at Austin, Austin, TX 78712, USA

5 Department of Civil Engineering, Cairo University, Giza 12613, Egypt

The combination of different binding and tendon materials led to the development of a number of anchor systems suitable to stabilize different geotechnical materials. Among the different systems, the grout bonded bar/tendon became the most commonly used type of soil anchors [27, 43]. Some grout-bar anchor systems are installed within the soil mass with no pretension, performing as passive supports. Such systems became known as soil nailing systems. A number of experimental as well as numerical investigations on these systems focused on the identification of relevant failure modes and load transfer mechanisms, which require good understanding of tendon–binder and binder–soil interface shear responses. In evaluating the performance of these anchor systems, these investigations have placed emphasis on the short-term (rapid loading) response under working stress conditions [4, 5, 8, 14, 15, 18–20, 23, 24, 31, 34, 39, 41, 47, 48, 58].

Unlike the abundance of previous studies on the short-term (rapid loading) response of grouted anchored systems, their long-term (creep) response has been significantly less investigated. The long-term response of reinforcement

systems such as geosynthetics, where the reinforcement itself is a material that exhibits rheological behavior has been the focus of a number of studies (e.g., [2, 35, 56, 60]). In addition, several other research studies have focused on the long-term (creep) response of anchor systems where the binder (e.g., epoxy binder) exhibits a rheological behavior [13, 25, 33, 36, 40, 42, 55]. An example involving a creep-induced failure is the collapse of the I-90 connector tunnel in Boston, Massachusetts, USA [38]. However, little information has been collected in the technical literature to understand the behavior of anchor systems where the soil where the anchor system is embedded exhibits rheological behavior (e.g., clay soils). This is probably because grouted anchored systems had previously been used mainly for temporary applications with a short service life (e.g., anchored shaft walls supporting excavations prior to backfill). The limited research previously conducted on the long-term behavior of grouted anchor systems embedded in clay soils include those reported by Hou and Li [21], Benmokrane and Ballivy [3], Gurinsky [17], and Xu et al. [54]. However, the information reported on the behavior of grouted anchor systems in clay soils has primarily focused on the pullout response of full-scale anchors involving complicated load transfer along the entire bond length, rather than on a systematic evaluation of interface behavior in particular with various conditions using element testing idea. The increasing use of grouted anchors in a number of geotechnical applications with comparatively long service life (e.g., anchored retaining wall stabilizing slopes) demands an understanding of the long-term (creep) behavior of grouted anchors, especially in systems used to reinforce clayey soils. The degree of saturation of the soil in which a grouted anchor is embedded was reported to influence the anchor's short-term interface shear response [5, 19, 46]. Additionally, the long-term properties of geomaterials are significantly affected by their moisture conditions [26, 29, 30]. Since soils adjacent to grout–soil interface are characterized by rheological properties [32, 37], it is reasonable to associate the creep behavior of grouted anchors in clayey soils with the moisture conditions of the surrounding soil zone, where the interface shear resistance of anchors is mobilized and a shear band develops. It should be noted that the moisture condition of the soil in which the anchor is embedded is related to the soil matric suction. While direct measurement of matric suction is comparatively complex, the creep behavior of grouted anchors could also be associated with the matric suction conditions of the surrounding soil zone. The effective stress state of the soils is largely affected by the varying matric suction, which would lead to different soil confinement around the anchor [1, 12]. However, since the soil moisture content is more frequently used in practice than the soil matric suction to describe soil conditions, soil

moisture content was adopted in this study to characterize the soil conditions affecting the interface behavior.

Pullout testing was adopted in this study to characterize the interface shear response of grouted anchors. Specifically, a comprehensive testing program was carried out using an element pullout cell that was specially designed to facilitate the preparation of grouted anchor specimens embedded in clayey soil placed at varying moisture and density conditions to examine their creep behavior. It should be noted that the element pullout cell involves a comparatively short embedment length, or bond length between the grouted anchor and the surrounding soil [9]. As indicated by findings from pullout tests on rock bolts [4, 34], the element testing conducted in this study was identified to be suitable to characterize the interface shear stress–displacement constitutive relationship by assuming uniformly distributed interface shear stresses along the grout–soil interface area [7, 11]. Ultimate short-term and long-term interface shear strength values of grouted anchors in clayey soils were obtained in tests conducted at varying degrees of saturation. In addition, the interface creep behavior of the tensioned soil anchor was characterized by a rheological model by developing correlations between interface shear stress and model parameters based on the generated experimental data.

2 Material properties

The test specimens prepared in this study were of cylindrical shape, involving a steel reinforcement bar placed at the central axis of each specimen surrounded by a cementitious grout slurry binder, which is in turn embedded within compacted clayey soil. The soil was collected from a flood plain along the Xiangjiang River, close to Hunan University, which is characterized by the presence of alluvial deposits. The collected soils were cleaned from foreign materials and mechanically pulverized, preserving only particles passing through the 5-mm sieve. The soil samples were mixed and sealed in plastic bags for 48 h to achieve an approximate uniform moisture distribution.

Laboratory tests were carried out in agreement with JTG E40-2007 (Test Methods of Soils for Highway Engineering, a Chinese standard [22]) to characterize the basic properties of the soil samples. These included characterization of the moisture content, soil density, specific gravity, plastic and liquid limits, particle-size distribution, and shear strength using direct shear tests. Figure 1 shows the soil particle-size distribution curve. Table 1 presents the properties of the soil, reinforcement, and grout materials involved in this study. It should be noted that values of physical and mechanical properties of soil samples were
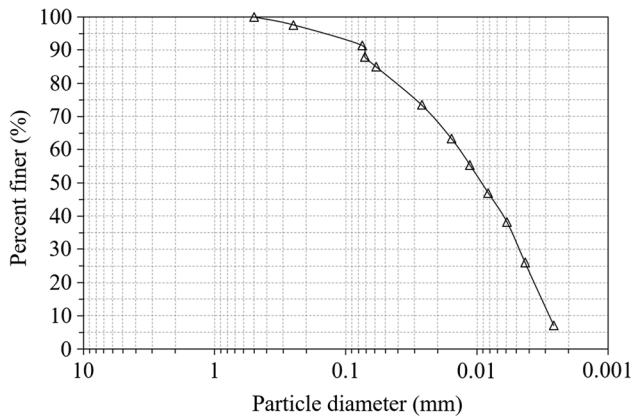
Fig. 1 Soil particle-size distribution

Table 1 Characteristics of the materials in element anchor cells

Properties/information	Value/description
Clayey soil	
Moisture content, w (%)	31.5
Dry density, ρ_d (g/cm^3)	14.5
Specific gravity, G_s	2.7
Liquid limit, LL (%)	45.2
Plasticity index, PI (%)	19.6
Average void ratio, e_0	1.1
Uniformity coefficient, C_u	4.9
Coefficient of curvature, C_c	0.6
Cohesion, c (kPa)	55.3
Internal friction angle, ϕ (°)	12.0
Reinforcement bar	
Type	Hot-rolled ribbed bar
Diameter, d_{bar} (mm)	8
Thread pitch, p_{bar} (mm)	5
Tensile strength, $\sigma_{t,bar}$ (MPa)	300
Tensile modulus, $E_{t,bar}$ (GPa)	230
Cementitious grout	
Sand type	Standard medium sand
Sand–cement–water ratio	1:1:0.45
Cement strength, $\sigma_{c,cement}$ (kPa)	42.5

tested with in situ soil conditions and would be changing in the process of specimen preparation.

3 Specimen preparation

As illustrated in Fig. 2, element-anchored soil specimens were prepared in three phases: compaction, grouting, and curing [9]. Soil samples were oven-dried under a temperature of 100 degrees centigrade for 24 h and were subsequently moisture conditioned to achieve an initial target moisture content of 16.0%. The conditioned samples were then placed in sealed plastic bags for over 24 h to ensure uniform moisture distribution within the soil samples. The soil samples were compacted in a compaction cell (Fig. 2a) in five lifts. Each lift was compacted with ten drops of a free-fall hammer to achieve the compaction energy of 592.2 kJ/m^3 (Fig. 2b). During the compaction process, a centralizer cased with a guide tube was placed in the center of the cell to orient the hammer and to allow placement of the reinforcement bar and grout binder. After compaction, the compaction setup was removed and the grouting setup was installed (Fig. 2c). In the grouting process, a reinforcement bar was placed at the center of the grouting hole (created by the presence of a guide tube during compaction), which was subsequently grouted by gravity. Simultaneously, an iron wire was used to densify the grout and to enhance its homogeneity. The samples were then placed in sealed plastic bags for 28 days for the grout to cure. It should be noted that the grouting hole was prepared during the compaction process, which differs from standard practice where grouting holes are drilled into native soils. Accordingly, drilling-induced disturbance to the surrounding clayey soils was not effectively controlled, and centralization of drilling hole is not guaranteed. On the other hand, the use of precast holes facilitated the preparation of consistent specimens, which was particularly appropriate for comparison of test results and allow a full release of the soil confining stresses around the anchor.

Figure 3 presents a schematic view of the element-grouted anchor specimen, showing the specimen dimensions. The base and cover plates of the pullout cell were used to constrain the soil displacement, rendering a fully fixed boundary on the top of the soil specimen moving upwards, making the anchor movement the only source of interface shear displacement [7, 11]. The diameter of the pullout cell is more than five times of the diameter of the cement grout, which was designed to minimize boundary effects that could be induced by the cell sidewall. Due to the all-around constraint that the pullout cell imposes on the soil, the soil volumetric deformation was assumed to be negligible throughout pullout testing. This assumption is based on the fact that soil dilatancy is minor under the shear stress level adopted in this testing program and that the soil volumetric deformation has been incorporated into the interface shear using this presented pullout setup [1, 59]. The diameter of the opening on the cover plate is 50 mm (Fig. 3b), while the diameter of the cement grout is 38 mm. As reported in previous evaluation of the pullout setup [7, 11], a diameter difference of 12 mm was selected to ensure that pullout failure develops at the interface rather than within the soil mass or the grout itself (as it could be the case for comparatively large or small opening
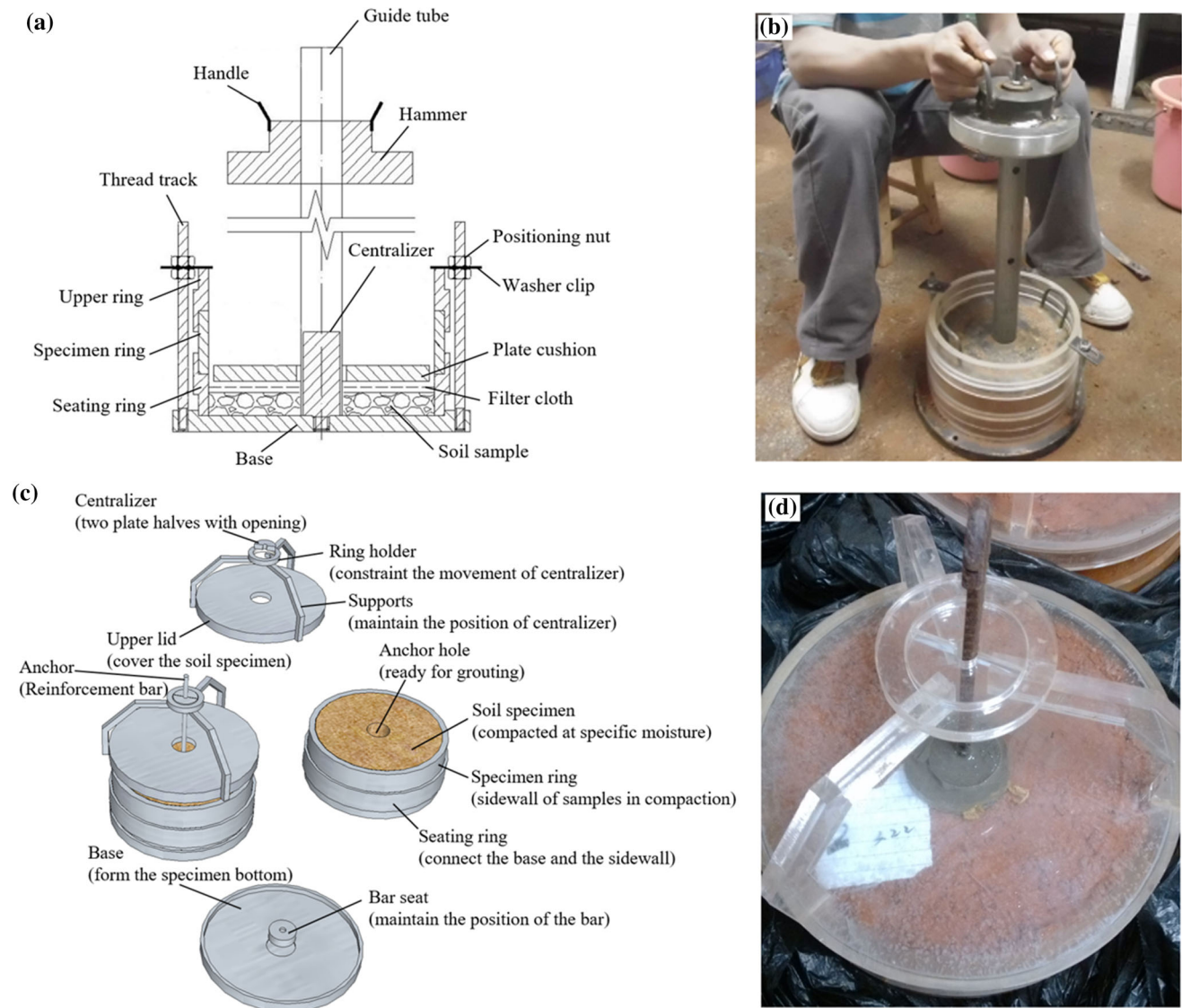
Fig. 2 Specimen preparation: **a** schematic of the compaction setup, **b** photograph of compaction setup, **c** schematic of the grouting setup, **d** photograph of grouting setup

sizes, respectively). The figure also shows the photographic view of an element-grouted anchor specimen. Note that the pullout cell with a completed specimen should be sealed with petroleum jelly between the cover plate and grouting in order to minimize moisture fluctuations during the pullout process.

4 Pullout testing program

The testing program is grouped into seven test series. Each series comprised of two identical specimens prepared simultaneously; one specimen was tested in short-term (rapid) pullout and the other was tested in long-term (creep) pullout. The moisture content varied among the series to investigate the influence of moisture condition on pullout response and the anchor–soil interface shear mechanisms. With respect to each test series, the short-term pullout test was conducted first to evaluate the ultimate pullout resistance, a value which was then used as a basis for the loading scheme for the creep pullout test that avoids specimens experiencing short-term pullout failure prior to exhibiting long-term pullout response.

4.1 Short-term pullout tests

The element-grouted anchor pullout setup (Fig. 4) was developed based on the Frictional Performance Testing System, available in the geotechnical engineering laboratory of Hunan University [10]. The reinforcement bar was
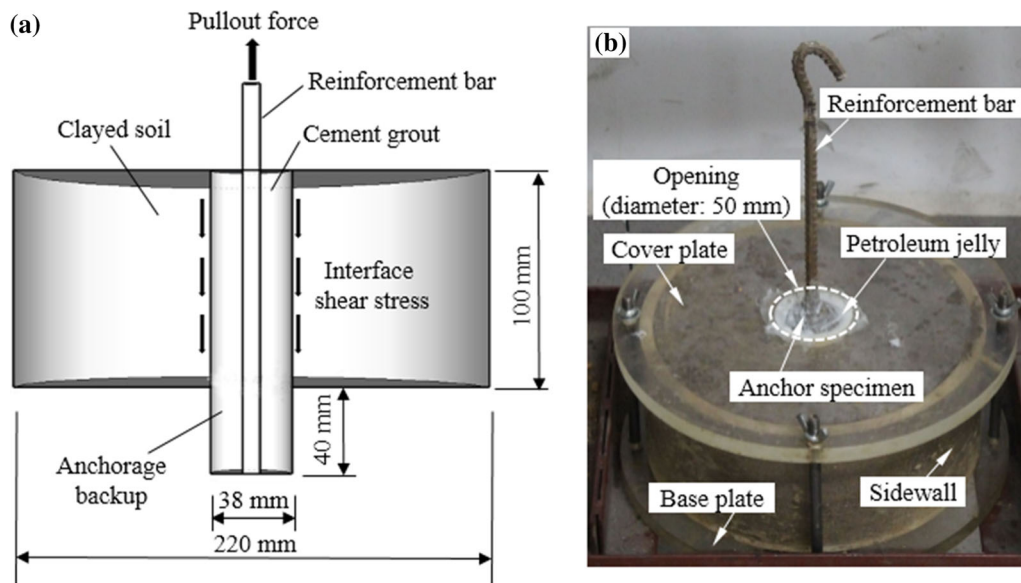
Fig. 3 Element-grouted anchor specimen: a schematic of specimen with dimensions, b view of setup of the pullout cell with specimen ready for testing
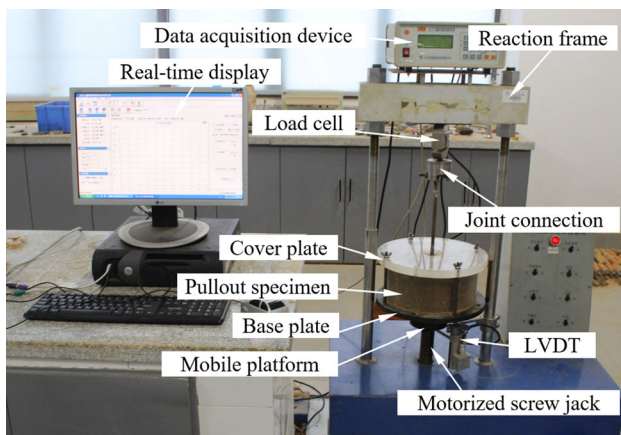

Fig. 4 Setup of instantaneous pullout testing device

attached to the reaction frame through a load cell and a joint connection. The pullout cell was fixed to a mobile platform controlled by a motorized screw jack. During the test, the platform was set to move downward at constant displacement rate of 1 mm/min. Real-time pullout force was recorded by the load cell, while real-time displacement of the platform was recorded by LVDT. Shear stresses and displacements along the anchor–soil interface were obtained assuming pseudo-static equilibrium of the reinforcement bar and relative displacement between the bar and the surrounding soil.

4.2 Long-term (creep) pullout tests

Creep pullout tests were carried out on a specially designed test setup (Fig. 5) using the second specimen of each test
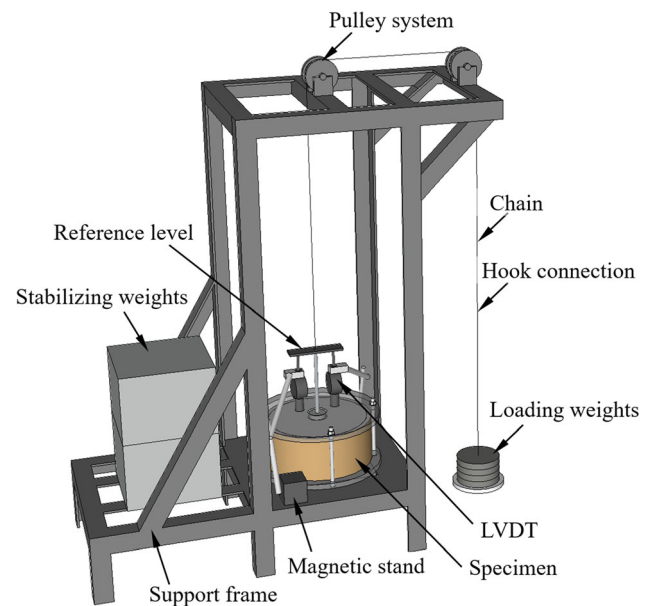

Fig. 5 Schematic of creep pullout testing setup

series. A multi-stage loading scheme was adopted in accordance with the Tan's method [50, 52] adopting as reference the ultimate pullout resistance N_{ult} obtained from the short-term pullout test for the companion test specimen (first specimen of each test series). A seating load in the range of 0.1 N_{ult} to 0.2 N_{ult} was initially applied to the specimen, followed by loading steps ranging from 0.10 to 0.15 N_{ult} to ensure that each specimen was tested at an adequate number of loading levels. The displacements at the anchor head (i.e., shear displacements) were monitored using LVDTs for each loading level. Once the anchor head

displacement rate at a given loading level dropped below 0.01 mm over 24 h, dead weights corresponding to the predefined loading step were added, initiating the subsequent loading level. Figure 6 displays views of exhumed grouted anchors as well as grout–soil interface and anchor head at pullout creep failure. A thin layer of the surrounding clayey soils could be observed as adhering to the grout surface, indicating the development of a shear band during pullout failure of grouted anchors. It should be noted that the thickness of the soil shear band that develops around the cement grout is likely affected by the diameter difference between the opening on the cover plate and the cement grout. Consequently, the thickness of the shear band was not quantified during the testing program. Interface shear failure was observed to occur consistently along the grout–soil interface, the shear resistance of which was far smaller than that of the bar–grout interface. Consequently, the term "anchor–soil interface" is used in this paper to represent the grout–soil interface, which usually corresponds to the weaker interface in grouted anchorage systems subjected to pullout loads.

5 Test results and analyses

5.1 Ultimate shear strength of anchor–soil interface

The relationship of the shear stress to shear displacement along the anchor–soil interface for specimens with varying moisture contents obtained from short-term pullout tests is presented in Fig. 7. Shear stresses were obtained by averaging the corresponding pullout forces along the entire interface area. This approach assumes a uniform distribution for the interface shear stresses, which is consistent
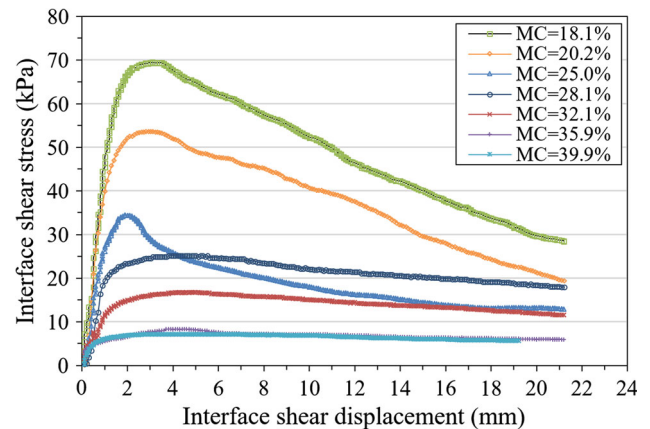

Fig. 7 Interface shear stress–displacement relationship obtained from short-term (rapid) pullout tests

with the element concept adopted in the design of the test [7, 11]. A strain softening response was observed for all specimens after the ultimate (peak) interface shear strength has been reached. Ultimate interface shear strength for specimens with different moisture contents (MC) is given in Table 2 and plotted in Fig. 8. The ultimate interface shear strength was found to decrease exponentially with increasing moisture content values of the soil where the anchor was embedded, at least for the range of moisture content values adopted in this study. It should be noted that the moisture contents of the specimens used in the short-term pullout tests may differ slightly from the moisture content of the specimens used in the long-term (creep) tests. Even though specimens of the same moisture content were prepared simultaneously, they may have slightly different moisture contents due to inherent variability during specimen preparation. Consequently, specimens of the same test series were characterized by the average value of their moisture content measurement results.
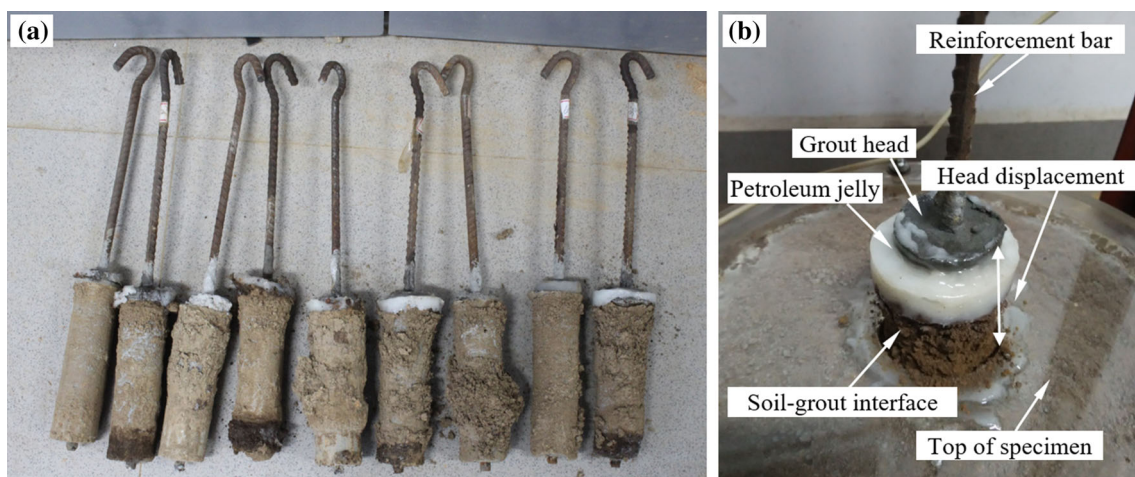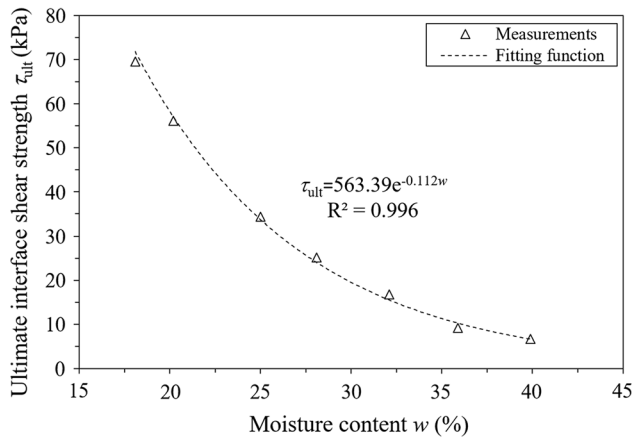

Fig. 6 Views of exhumed grouted anchors: **a** grout–soil interfaces, **b** grout head

Table 2 Ultimate shear strength of anchor–soil interfaces versus moisture content

Moisture content w (%)	18.1	20.2	25.0	28.1	32.1	35.9	39.9
Ultimate interface shear strength τ_{ult} (kPa)	69.56	56.15	34.36	25.14	16.76	9.22	6.70

$$\tau_{ult} = 563.39 e^{-0.112w}$$
$$R^2 = 0.996$$

Fig. 8 Ultimate interface shear strength versus moisture content

## 5.2 Effect of moisture content on creep results

Figure 9 shows the time history of interface shear displacement as obtained during multi-stage pullout loading of specimens prepared with increasing values of initial moisture content. The sharp displacement increases observed in the time history results correspond to the onset of a loading stage. Each loading stage was labeled by the corresponding stress level (SL), or the ratio of the pullout shear stress applied in the loading stage to the ultimate interface shear strength (as obtained from the short-term pullout test results). The experimental approach adopted in this investigation allowed the generation of multiple creep curves (one per loading stage) using a single grouted anchor specimen and subjecting it to increasing constant stress levels. This approach was adopted partly because it minimizes inconsistencies of experimental results that have often been reported when adopting multiple specimens to generate the several constant stress levels in a creep testing program. Specifically, the approach allowed adopting nonlinear superposition techniques [51], to transform the multi-stage time history shown in Fig. 9 for each moisture content (left-hand side of Fig. 9a through g) into multiple creep curves, with each curve corresponding to constant stress levels (right-hand side of Fig. 9a through g).

As illustrated by creep curves obtained at various stress levels (Fig. 9), the shear displacement–time relationships obtained under constant load can be generally described using three phases that are typically manifested in the creep response of many materials. Figure 10 illustrates a typical creep curve, where the primary creep phase is characterized by an initially decreasing creep rate. As suggested by the family of creep curves for specimens with the same moisture contents in Fig. 9, both the curvature of the primary creep phase and the time corresponding to the onset of the secondary creep phase show an increasing trend with increasing stress level. The secondary creep phase is identified by steady creep rate, which also corresponds to the lowest creep rate in the entire creep curve. As shown by the creep curves corresponding to the first and second loading stages in Fig. 9, comparatively low stress levels led to a negligible deformation rate due to creep flow. The tertiary creep phase is characterized by an increasing creep rate, ultimately leading to creep rupture. Failure is often characterized as the onset of the tertiary creep phase, as illustrated in Fig. 10. Because interface shear failure has developed over the entire length of the anchor by the time corresponding to the onset of tertiary creep phase, comparatively short periods of time, ranging from 0.5 to 0.7 h, characterized the time corresponding to tertiary creep phase in the tests conducted as part of this investigation. It should be noted that the presence of the tertiary creep phase was affected not only by the magnitude of the applied stress level but also by the moisture content of the soil in which the grouted anchor system was embedded.

The development of a tertiary creep phase occurred for the highest stress level adopted in all specimens tested in this investigation. It should be noted that, for the creep curves under the highest stress levels in specimens with comparatively high moisture contents (Fig. 9e–g), the primary and secondary creep phases occurred within a very small shear displacement range, with only tertiary creep phase being distinctly observed. The transition from the secondary creep phase to the tertiary creep phase can be associated with the occurrence of pullout creep failure along the anchor–soil interface.

5.3 Long-term shear strength of anchor–soil interface

The interpretation of creep data has often been conducted by developing isochronous curves, as they allow determination of long-term displacements and long-term strength of geotechnical systems (e.g., [28, 29, 45, 51]). The use of isochronous curves was adopted in this study to evaluate the long-term shear strength of anchor–soil interfaces. An isochronous curve plots the creep displacements and stresses corresponding to a given time period since the
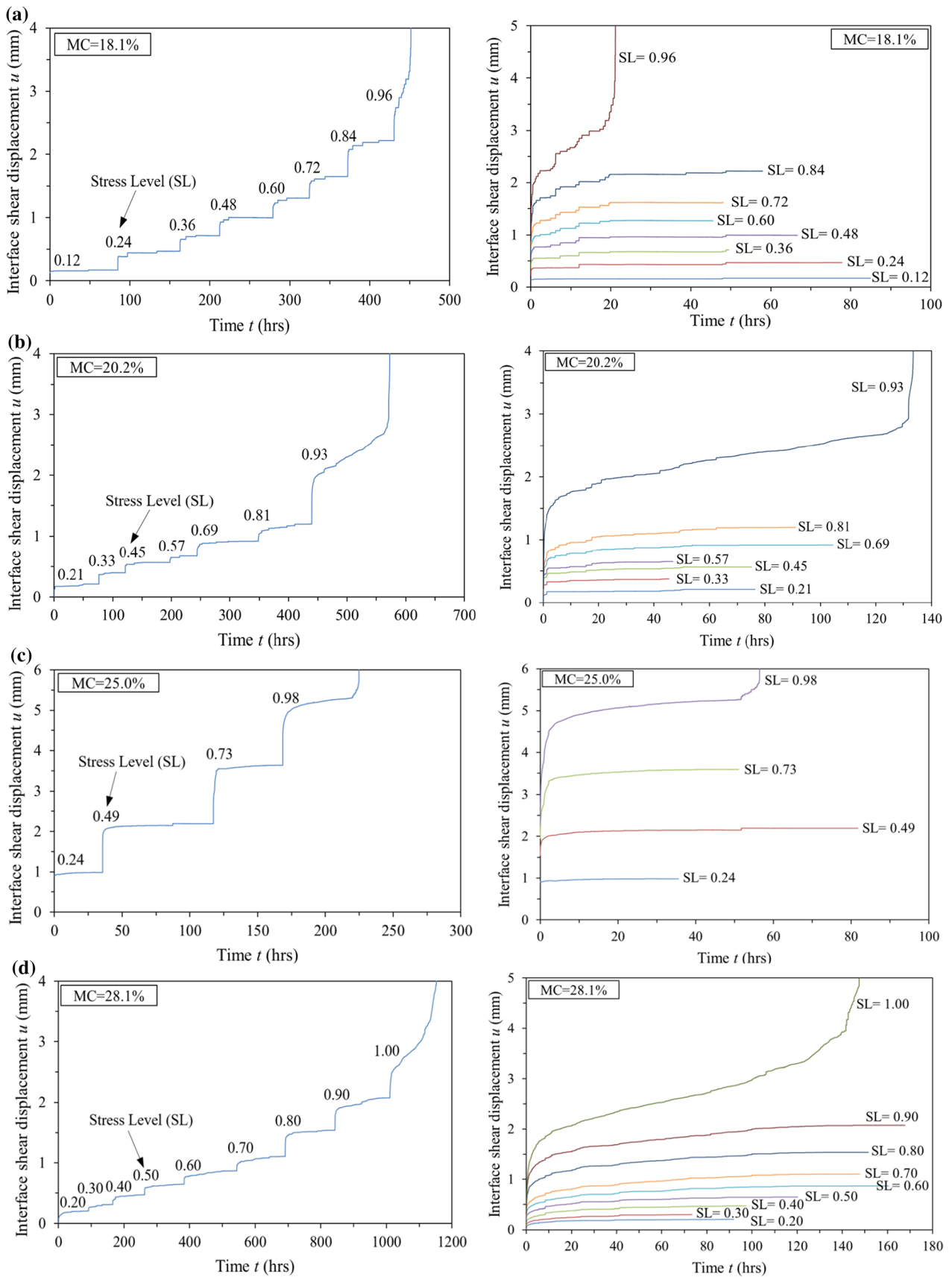
◀**Fig. 9** Multi-stage time history and creep curves for specimens of different moisture contents: **a** MC = 18.1%, **b** MC = 20.2%, **c** MC = 25.0%, **d** MC = 28.1%, **e** MC = 32.1%, **f** MC = 35.9%, **g** MC = 39.9%

initiation of creep loading. Specifically, in shear displacement–time space (Fig. 9), the displacements and corresponding stress level that can be obtained at a given time from the creep curves can be used to define a family of shear stress–displacement curves that correspond to a

single period of time (i.e., isochronous curves), as shown in Fig. 10. The inflection point in an isochronous curve, i.e., the transition from elastic to elastoplastic behavior, was adopted to identify the onset of interface creep damage. The loci defined by the inflection points on different isochronous curves in the shear stress–displacement space tend to correspond to a constant stress value. This constant stress is adopted as the long-term interface strength of the anchor–soil specimen. The inflection points and long-term shear strength values are shown in Fig. 11. Table 3 also
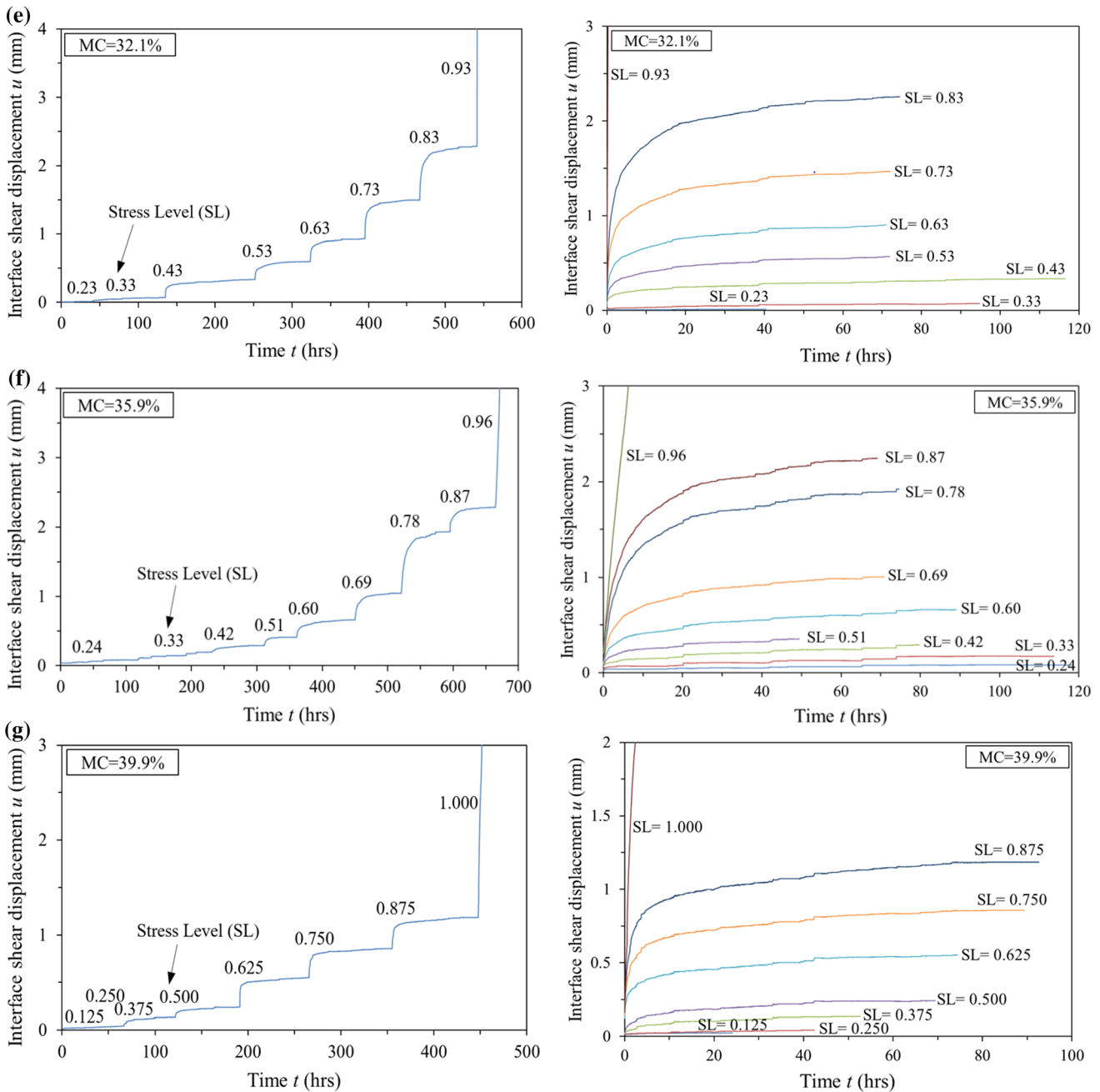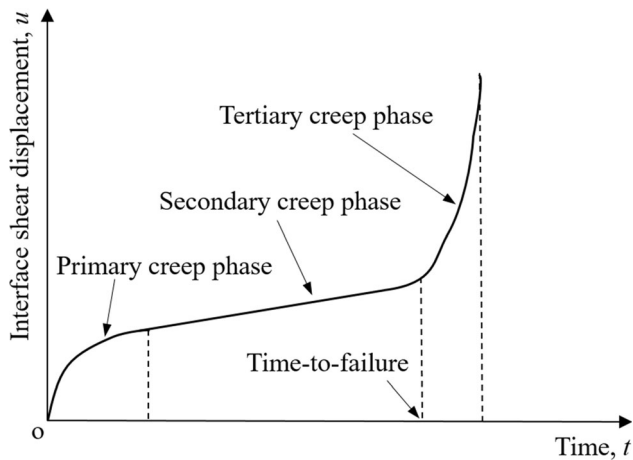

Fig. 9 continued

Fig. 10 Typical creep curve, showing three creep phases

summarizes the long-term strength of anchor–soil interface for specimens of increasing values of moisture content.

The interface shear creep response exhibited a highly nonlinear response, as indicated by the evolution of shear stress–displacement curve with time (i.e., isochronous curves). The slopes of the isochronous curves were observed to decrease with increasing creep time. The relatively high impact of creep time on the stiffness of the isochronous curves presented in Fig. 11 can be used to characterize the evolution of rheological deformations on the anchor–soil interface.

Examination of the displacements corresponding to a constant stress level as obtained from a family of isochronous curves (Fig. 11) reveals the onset of the different creep phases in the system. Specifically, the shear displacements between consecutive isochronous curves are constant, while the grouted anchor is undergoing secondary creep phase, while such shear displacements between consecutive isochronous curves decrease and increase during the primary and tertiary creep phases, respectively. That is, the convergence of consecutive isochronous curves over time (i.e., a decreasing difference in shear displacement for a given stress level) corresponds to primary creep phase, while the divergence of consecutive isochronous curves with time (i.e., increasing difference in shear displacements for a given stress level) corresponds to tertiary creep phase.

The transitional creep method, commonly adopted in the characterization of rock rheology, was employed to examine the adequacy of the long-term shear strength values obtained in this study. According to this method, the maximum stress applied to specimens (specifically the anchor–soil interface in this testing program) that exhibit secondary creep phase corresponds to the long-term strength. Creep displacements develop at a decreasing rate until they stabilize at a constant rate when the external

shear stress applied to the interface is smaller than the long-term shear strength. Otherwise, when the external shear stress applied to the interface reaches the long-term shear strength, the interface yields until creep failure occurs, manifested by the development of tertiary creep phase (i.e., increasing creep rate). In other words, the long-term strength corresponds to a specific external stress that induces the transition from the absence to the presence of tertiary creep phase observed in the family of creep curves under varying stress levels.

Although the number of external stress levels adopted in the creep testing program conducted as part of this study was significant, the exact transitional stress falls within the range of two consecutive applied stress levels, referred to herein as the transitional range (TR). This transitional range can be identified by examining the changes in the creep rate as measured at the end of stage (i.e., the creep rate at the end of the creep curves shown in Fig. 9) for the different loading levels corresponding to each stage, as shown in Fig. 12. The sharp increase in the end-of-stage creep rate from a secondary creep phase in a loading level to a tertiary creep phase in the succeeding loading level corresponds to the range of stress levels that includes the long-term shear strength. This is because failure would have fully developed along the interface for the case of an imposed interface shear stress that exceeds the long-term strength. In contrast, partial or progressive failure would have developed along the interface for cases in which the end-of-stage creep rates between two successive loading levels do not differ significantly, indicating that the long-term shear strength has not been exceeded. A similar approach to validate the determination of the long-term shear strength using isochronous curves was reported by Liu and Xu [28] as part of research on the characterization of rock strength. For example, a significant increase in the end-of-stage creep rate was observed for the specimen with 18.1% moisture content through comparison with previous increases, from the sixth loading stage to the seventh, indicating a transition from secondary to tertiary creep phases in this range (i.e., creep failure has occurred or long-term strength has reached). Transitional ranges for specimens with different moisture contents were also defined in terms of dimensionless stress levels, as presented in Fig. 12.

A reduction factor is introduced in this study as the ratio between the long-term interface shear strength and the ultimate interface shear strength (Table 4). Overall, the obtained long-term interface shear strength values were
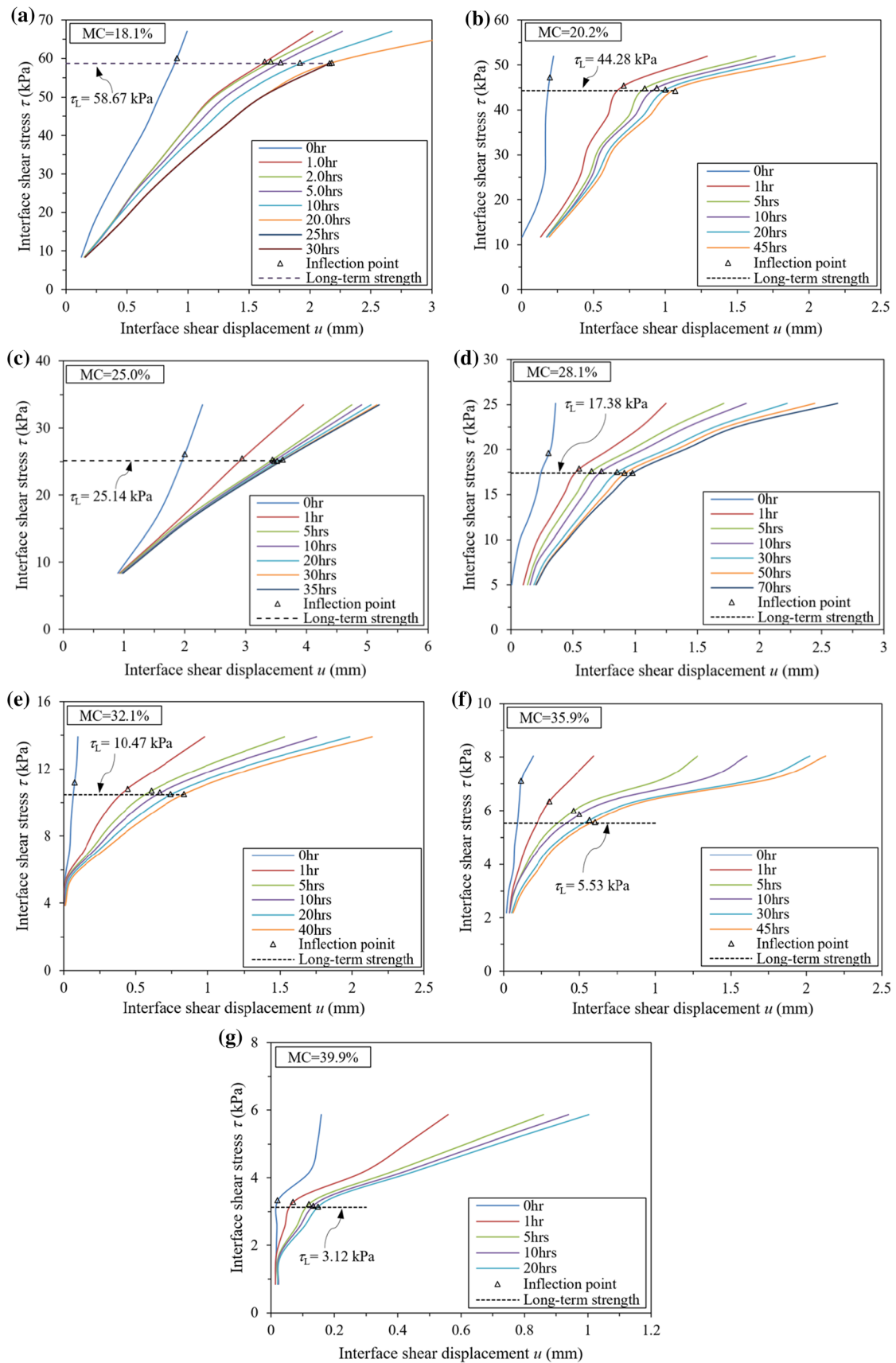
Table 3 Long-term shear strength of anchor–soil interface versus moisture content

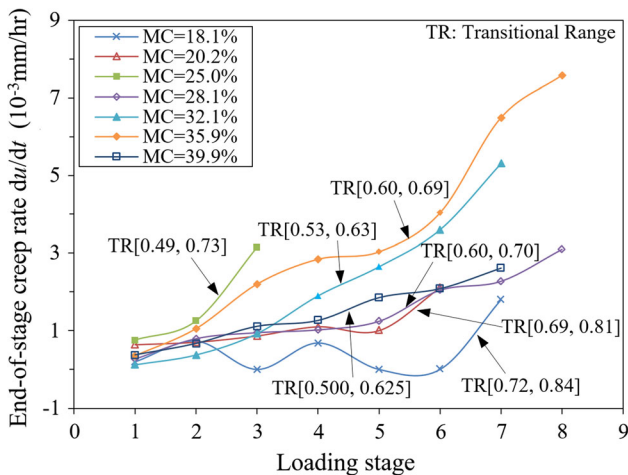| Moisture content w (%)	18.1	20.2	25	28.1	32.2	35.9	39.9
Long-term shear strength τ_L (kPa)	58.67	44.28	25.14	17.38	10.47	5.53	3.12

Fig. 12 End-of-stage creep rate with increasing loading stages for specimens with varying moisture conditions

Table 4 Shear strength reduction factors for anchor–soil interfaces with increasing moisture content

Parameters	Values						
Moisture content w (%)	18.1	20.2	25	28.1	32.2	35.9	39.9
Ultimate shear strength τ_{ult} (kPa)	69.56	56.15	34.36	25.14	16.76	9.22	6.70
Long-term shear strength τ_L (kPa)	58.67	44.28	25.14	17.38	10.47	5.53	3.12
Reduction factor R_f	0.84	0.79	0.73	0.69	0.62	0.60	0.47

found to be within the transitional ranges identified for the different specimens. This confirms the suitability of the techniques adopted to determine the long-term shear strength for anchor–soil interfaces via multi-stage loading pullout creep testing.

Figure 13 shows the reduction factors for the anchor–soil interface shear strength versus moisture content of surrounding soils. The reduction factors were found to
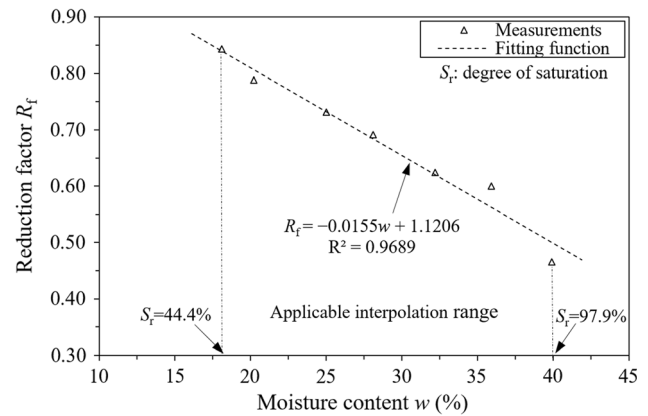

Fig. 13 Interface shear strength degradation factor versus moisture content of encapsulating soil

decrease linearly with increasing soil moisture content, which can be fitted using the linear function also shown in Fig. 13. Once the ultimate anchor–soil interface strength has been characterized using short-term (rapid) load tests, the linear relationship shown in Fig. 13 is useful to predict the long-term interface shear strength for a given soil moisture condition. With the determination of the relationship between reduction factor and moisture content, the design of grouted anchors and anchored structures with a long service life would be simplified considerably for engineers, eliminating the need for special creep tests. However, use of such linear relationship is justified only within the range of moisture content values adopted in this testing program (e.g., 18.1 to 39.9% in this case), corresponding to degrees of saturation ranging from 44.4 to 97.9%, respectively. It should be noted that the aforementioned linear relationship was derived based on test results of the specific clayey soils adopted in this study. While the general trends may be useful to understand the impact of soil moisture content, site-specific correlations would be necessary for projects involving other clayey soils.

6 Rheological model of pullout creep response for grouted anchors in clayey soils

Burgers model, which involves a combination of the Kelvin–Voigt and Maxwell models in series, has been used extensively to characterize the pullout creep response of anchors. However, its applicability has been limited to creep curves characterized by a linear tertiary creep phase [25]. The Kelvin–Voigt model has been recognized as a suitable approach to predict creep behavior, with predicted strains approaching a constant value with increasing time. On the other hand, the Maxwell model has been primarily

used to represent the strain as a linear function of time [49, 57]. The viscoelastoplastic damage element based on Kachanov's law of damage development used to evaluate rock rheology is reportedly capable of characterizing both the linearly brittle tertiary creep phase of hard rock and the nonlinear tertiary creep phase of soft rock [6, 44]. Consequently, the Burges model was modified by replacing the Maxwell model by a second Kelvin–Voigt model (resulting in two Kelvin–Voigt models in series) and further improving it by introducing the damage element, resulting in a hybrid model. This hybrid model consists of two components connected in series: a damage element and a generalized Kelvin model, as illustrated in Fig. 14. The model is then capable of accounting for the nonlinearity of the tertiary creep phase, as observed in the creep curves obtained in this testing program (Fig. 9).

The total interface shear displacement u can be determined by adding a viscoelastoplastic component defined by the damage element u_{de} and the viscoelastic component defined by the generalized Kelvin–Voigt model u_k as follows:

$$u = u_{de} + u_K \tag{1}$$

The time-dependent elastoplastic displacement component u_{de} defined by the damage element can be established as follows:

$$u_{de} = \begin{cases} \dfrac{\tau}{E_0} & \tau < \tau_L \\ \dfrac{\tau}{E_0}\left(1 - \dfrac{t}{t_F}\right)^{-\alpha} & \tau \geq \tau_L \end{cases} \tag{2}$$

where τ is the shear stress on anchor–soil interface; τ_L is the long-term shear strength of anchor–soil interface; t_F is the time to failure (i.e., the time corresponding to the onset of the tertiary creep phase); E_0 is the Young's modulus of the damage element; α is an exponential parameter; and t is the pullout creep time.

The shear displacement corresponding to the viscoelastic component u_k can be expressed as follows:

$$u_K = \frac{\tau}{E_1}\left[1 - \exp\left(-\frac{E_1}{\eta_1}t\right)\right] + \frac{\tau}{E_2}\left[1 - \exp\left(-\frac{E_2}{\eta_2}t\right)\right] \tag{3}$$

Damage element

Generalized Kelvin-Voigt model

Fig. 14 Hybrid model for characterizing creep behavior of anchor–soil interface

where E_1 and E_2 are the Young's moduli of spring elements; η_1 and η_2 are the coefficients of viscosity of dashpot elements, in the generalized Kelvin–Voigt model.

A switch function $\langle\tau_0\rangle$ is introduced as follows:

$$\langle\tau_0\rangle = \begin{cases} 0 & \tau < \tau_L \\ 1 & \tau \geq \tau_L \end{cases} \tag{4}$$

Equation (1) can be rewritten in a general form as follows:

$$u = \frac{\tau}{E_0}\left(1 - \frac{\langle\tau_0\rangle t}{t_F}\right)^{-\alpha} + \frac{\tau}{E_1}\left[1 - \exp\left(-\frac{E_1}{\eta_1}t\right)\right] + \frac{\tau}{E_2}\left[1 - \exp\left(-\frac{E_2}{\eta_2}t\right)\right] \tag{5}$$
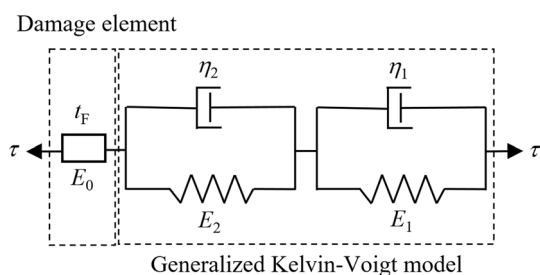
7 Discussion

The pullout creep response of the anchor–soil interface for grouted anchors embedded in moisture-conditioned clayey soils and subjected to sustained pullout force (constant stress level) was fitted using the proposed hybrid rheological model, as previously discussed. Figure 15 illustrates the fitting curves of the experimental data as obtained from the pullout creep test for the one of the specimens in the experimental program (prepared with an 18.1% moisture content). Equally good fitting curves were also obtained using experimental data generated from the specimens prepared at other moisture contents.

Table 5 presents the values of the parameters corresponding to the hybrid model and the coefficient of determination R^2 obtained in fitting the experimental creep data for the different stress levels adopted for the creep curves generated using a moisture content of 18.1%. The fitting for all the creep curves is particularly good, as established by the coefficients of determination, which exceed 94% for all stress levels considered in this study.
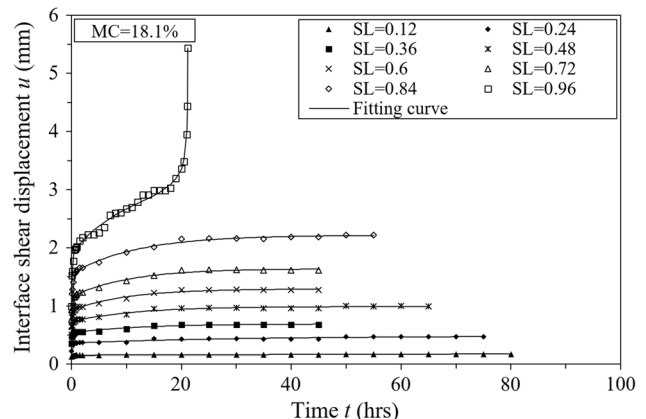

Fig. 15 Data fitting using the proposed hybrid model

Table 5 Hybrid model parameters for specimen with moisture content of 18.1%

Hybrid model	$u = \frac{\tau}{E_0}\left(1 - \frac{\langle\tau_0\rangle t}{t_F}\right)^{-\alpha} + \frac{\tau}{E_1}\left[1 - \exp\left(-\frac{E_1}{\eta_1}t\right)\right] + \frac{\tau}{E_2}\left[1 - \exp\left(-\frac{E_2}{\eta_2}t\right)\right]$							
	Stress level (SL)							
Parameter (unit)	0.12	0.24	0.36	0.48	0.60	0.72	0.84	0.96
E_0 (kPa)	65	75	71	66	63	64	64	68
E_1 (kPa)	350	136	160	149	161	134	93	60
η_1 (kPa h)	30,846	4105	1887	1530	1120	1067	1033	507
E_2 (kPa)	58	125	143	131	113	103	88	60
η_2 (kPa h)	128	8	14	21	25	30	18	9
t_F (h)	n/a	n/a	n/a	n/a	n/a	n/a	n/a	21.16
α	n/a	n/a	n/a	n/a	n/a	n/a	n/a	0.17
R^2	0.94	0.96	0.98	0.98	0.99	0.99	0.99	0.97

n/a, not applicable

Table 6 Hybrid model parameters for specimen with moisture content of 28.1%

Hybrid model	$u = \frac{\tau}{E_0}\left(1 - \frac{\langle\tau_0\rangle t}{t_F}\right)^{-\alpha} + \frac{\tau}{E_1}\left[1 - \exp\left(-\frac{E_1}{\eta_1}t\right)\right] + \frac{\tau}{E_2}\left[1 - \exp\left(-\frac{E_2}{\eta_2}t\right)\right]$								
Parameter (unit)	Stress level (SL)								
	Fitting							Prediction	
	0.2	0.3	0.5	0.6	0.7	0.9	1.0	0.4	0.8
E_0 (kPa)	454	183	77	60	59	53	70	99	61
Correlation	$E_0 = 3999.03\mathrm{e}^{-11.59(\mathrm{SL})} + 60.22; R^2 = 0.999$								
E_1 (kPa)	46	47	40	37	32	27	24	42	30
Correlation	$E_1 = -29.80(\mathrm{SL}) + 54.06; R^2 = 0.956$								
η_1 (kPa h)	589	581	899	1380	1385	1461	2371	914	1624
Correlation	$\eta_1 = 1774.62(\mathrm{SL}) + 204.09; R^2 = 0.816$								
E_2 (kPa)	61	74	79	70	63	26	18	76	50
Correlation	$E_2 = -206.61(\mathrm{SL})^2 + 184.08(\mathrm{SL}) + 35.13; R^2 = 0.952$								
η_2 (kPa h)	13	14	17	34	31	18	17	14	18
Correlation	$\eta_2 = 5.33 \times 10^{-12}\mathrm{e}^{\left[-115.83(\mathrm{SL})^2 + 148.47(\mathrm{SL}) - 18.51\right]} + 5.62(\mathrm{SL}) + 12.09; R^2 = 0.981$								
t_F (h)	n/a	n/a	n/a	n/a	n/a	n/a	147.9	n/a	n/a
α	n/a	n/a	n/a	n/a	n/a	n/a	0.158	n/a	n/a

n/a, not applicable

The predicting capability of the hybrid model was evaluated for the case of moisture content of 28.1%. Because a group of governing parameters for the hybrid model can be obtained for each loading stress using the creep data measured under this stress, the stress-dependency of all governing parameters was emphasized in this evaluation. Specifically, creep data measured under stress levels of 0.2, 0.3, 0.5, 0.6, 0.7, 0.9, and 1.0 were used in fitting to derive governing parameters of hybrid model corresponding to each stress level as shown in Table 6. Correlation of each governing parameter and the stress

level (i.e., stress-dependency of model parameters) was further developed using these parameters obtained in fitting as shown in Fig. 16. The formulae of fitting functions for hybrid model parameters are presented in Table 6. The stress-dependency correlations of model parameters were subsequently adopted to define the governing parameters of hybrid model for stress levels of 0.4 and 0.8, as well as the corresponding creep curves at the two stress levels predicted on basis of the hybrid model.

Values of nine groups of model parameters corresponding to nine stress levels (seven groups obtained in
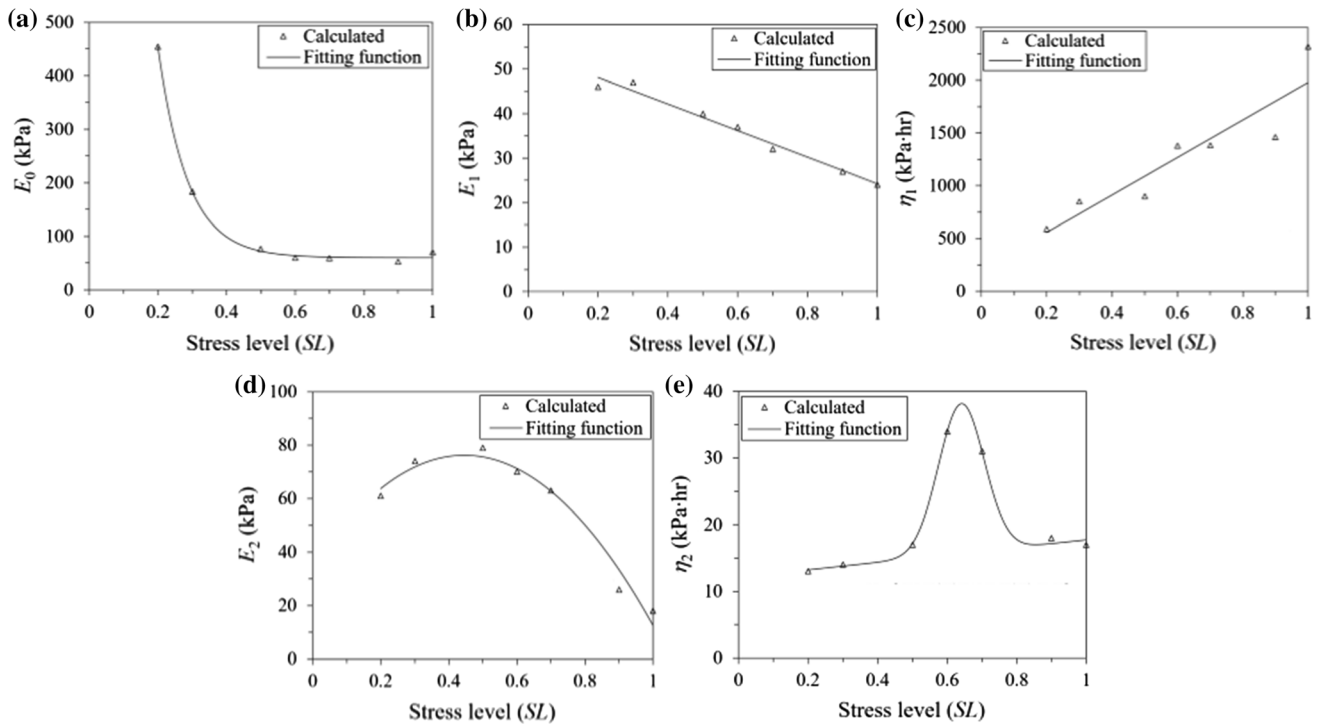
Fig. 16 Stress-dependency of hybrid model parameters: **a** E_0, **b** E_1, **c** η_1, **d** E_2, **e** η_2
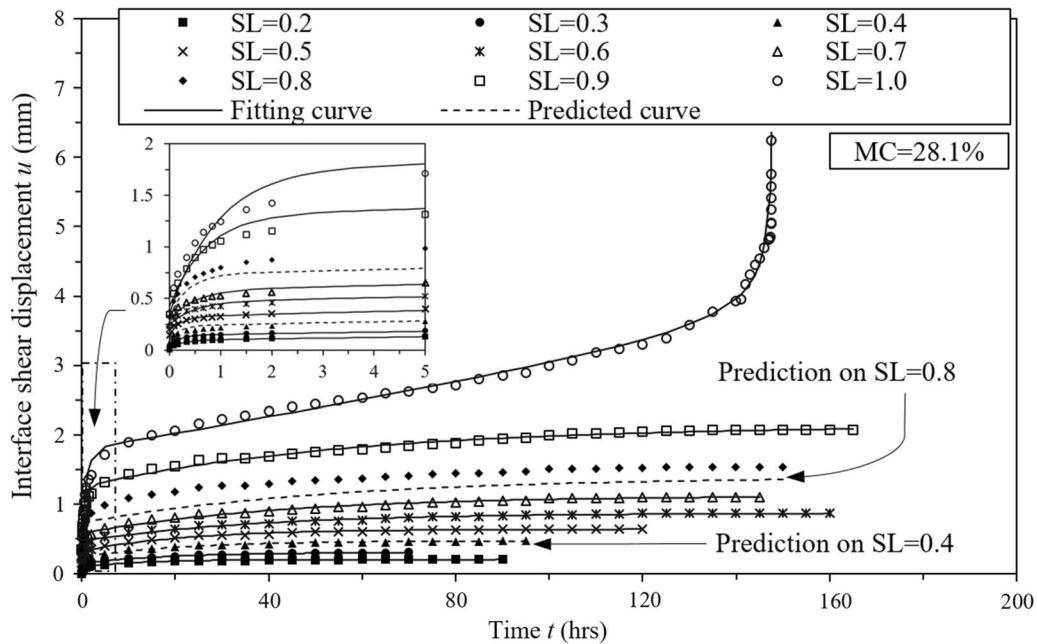

Fig. 17 Hybrid model fitting and prediction for the case of soil moisture content of 28.1%

fitting using hybrid model and two groups defined in prediction using stress-dependency correlations) are presented in Table 6. It is noteworthy that only correlations for elastic moduli and viscosity coefficients involved in the generalized Kelvin–Voigt model were derived in fitting, and correlations for model parameters defined in the damage element (i.e., t_F and α) were not available. It is because that the two parameters were only used in fitting on the creep data corresponding to the highest stress level (as distinguished from other stress levels using "n/a" in Tables 5 and 6) which was characterized by the presence of tertiary creep phase.
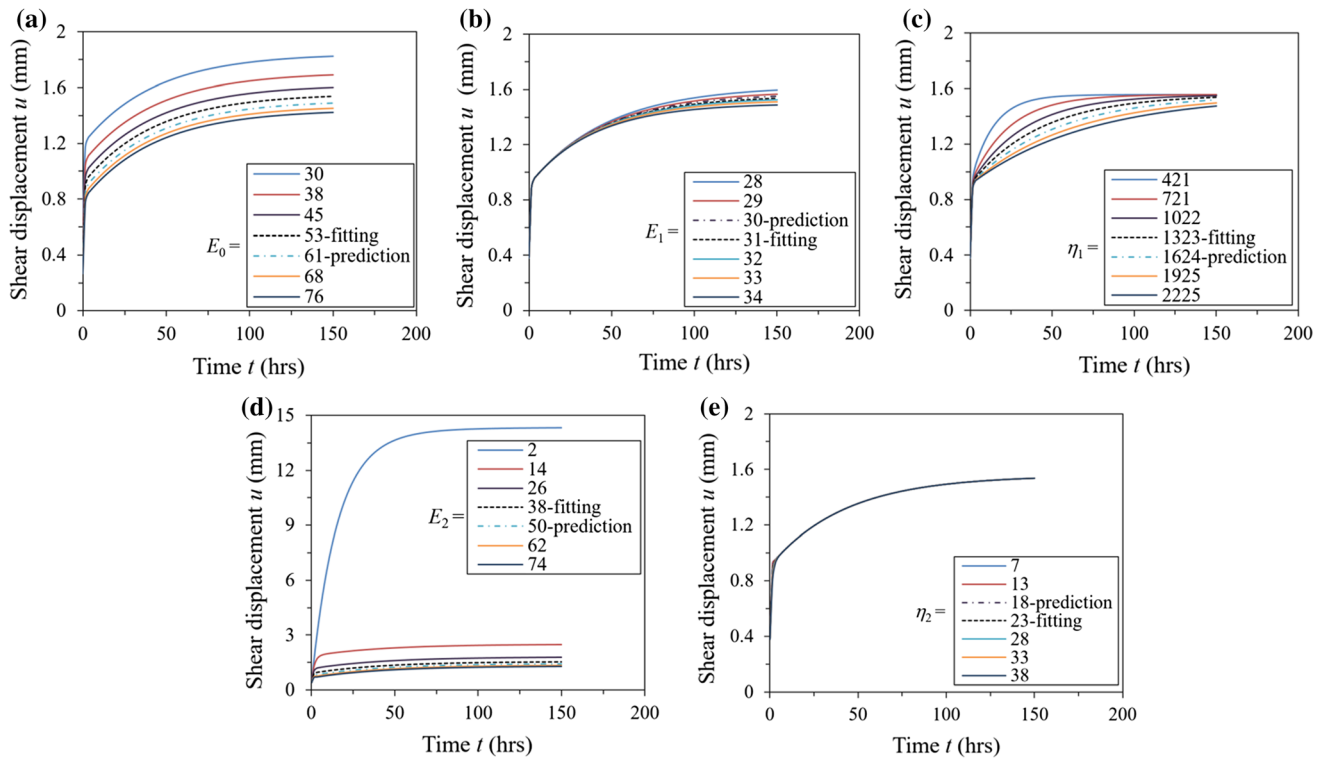
Fig. 18 Influence of model parameters on creep response with steps of prediction-fitting residual: **a** E_0, **b** E_1, **c** η_1, **d** E_2, **e** η_2

Table 7 Variation of model parameters based on prediction-fitting residual

Parameters	E_0 (kPa)	E_1 (kPa)	η_1 (kPa h)	E_2 (kPa)	η_2 (kPa h)
Prediction (P)	61	30	1624	50	18
Fitting (F)	53	31	1323	38	23
Residual (ρ)	8	1	301	12	5
$F - 3 \times \rho$	30	28	421	2	7
$F - 2 \times \rho$	38	29	721	14	13
$F - 1 \times \rho$	45	30	1022	26	18
$F + 0 \times \rho$	53	31	1323	38	23
$F + 1 \times \rho$	61	32	1624	50	28
$F + 2 \times \rho$	68	33	1925	62	33
$F + 3 \times \rho$	76	34	2225	74	39

The hybrid model-based predicted creep curves for stress levels of 0.4 and 0.8 were compared with the corresponding measurements, along with the fitting curves for remaining stress levels, as shown in Fig. 17. As shown in the figure, the model predictions for a stress level of 0.4 agree well with the experimental data, while the predictions for a stress level 0.8 deviated from experimental data with comparatively smaller shear displacements. This discrepancy can be attributed to differences with model

parameters corresponding to the stress-dependency correlations, which were derived by fitting a limited number of stress levels, as shown in Fig. 16. Additionally, the derived correlations are empirical best fits, which could be improved with more data generated from tests conducted at additional levels of testing variables to those used in the testing program.

In order to assess the prediction effectiveness, the hybrid model parameters predicted from the different correlations were compared against those resulting from fitting experimental data, typically for stress level 0.8, with emphasis on the prediction-induced residual for the various parameters. Figure 18 shows the influence of the prediction fitting residual for each model parameter on the predicted creep response by extending parameter values in a parametric analysis with these residuals as steps, as shown in Table 7.

A parametric analysis was conducted by extending each parameter by plus/minus three times the prediction-fitting residual in relation to the baseline value for each parameter. The sensitivity of the predicted creep response using the hybrid model for the prediction-fitting residual of each model parameter was observed to show significant differences as shown in Fig. 18. Varying the residual of E_0 results in a transition of the creep curve without modifying its shape, because E_0 is independent of time in the hybrid model. Varying the residual of E_1 does not result in

different creep curves up to 50 h, which is almost one-third of the total creep time used in this testing program. Varying the residual of η_1 leads to the change in the curvature of the creep curve (also characterized by the turning point from primary creep phase to secondary creep phase), but has essentially no impact on the end-of-stage creep displacement (i.e., the steady shear displacement level to which all creep curves tend to converge in Fig. 18c). The stress-dependency correlation of η_1 obtained from fittings under seven stress levels was unable to adequately representing the relationship between η_1 and stress level (as indicated by the comparatively low coefficient of determination in Table 6), but this deficiency would not induce significant derivation of ultimate creep displacement in predictions using this correlation. The creep curves were found to be generally not influenced by varying the residual of η_2, but it was highly sensitive to varying the residual of E_2. More cautions are required in using of the correlation of E_2 and stress level than that of η_2 and stress level to predict the creep response. It is consequently justified to use a correlation of η_2 with lower determination coefficient but simper expression which manifests very complicated in the present correlation. It is observed that the plus residual step for all model parameters involved in Fig. 18 tends to result in less discrepancies between the neighboring predicted creep curves than that for the minus residual step. It implies that the underestimated model parameters using these correlations should be avoided with more concerns than that of overestimated ones in predicting creep response based on the stress-dependency hybrid model.

The rheological hybrid model was confirmed as able to account for stress-dependency and suitable to characterize the anchor–soil interface shear creep behavior for grouted anchors subjected to pullout loading in clayey soils. The model was also able to account for the significant impact of the clay moisture content on the creep response of the grouted anchor system. Specifically, the prediction effectiveness of the hybrid model was examined using data generated during pullout creep tests, and the impact of prediction-fitting residual for each model parameter on the creep response was evaluated.

8 Summary and conclusions

Element creep pullout tests were carried out in a specially designed grouted anchor element pullout cell, with loading levels defined using as reference the ultimate pullout resistance measured in a series of companion short-term (rapid loading) pullout tests. To examine the influence of moisture conditions on the anchor–soil interface's shear creep behavior, grouted anchor element specimens were embedded in moisture conditioned clayey soils. The long-term shear strength of the anchor–soil interface was determined with varying moisture contents by adapting rheology methods previously used to characterize other geotechnical systems. A rheological hybrid model was used to characterize the pullout creep response of grouted anchors embedded in clayey soils. The stress-dependency correlations for model parameters were evaluated based on fittings of measurements from creep pullout tests. The following conclusions can be drawn from this investigation:

- The ultimate shear strength values of anchor–soil interfaces obtained in short-term (rapid loading) pullout tests were found to decrease exponentially with increasing moisture contents of the soil where the anchors are embedded.
- The tertiary creep phase was observed in creep curves where the shear stress applied to the anchor–soil interface exceeded its long-term interface shear strength. Otherwise, only primary and secondary creep phases were observed in the system creep response.
- An interface shear strength reduction factors (i.e., ratio of the long-term shear strength to the ultimate shear strength) for anchor–soil interface was found to decrease linearly with increasing moisture content of the soil where the grouted anchor is embedded.
- A rheological hybrid model comprising of two Kevin–Voigt models and a damage element connected in series was found to adequately characterize the creep behavior of a grouted anchors in clayey soils, especially the nonlinear tertiary creep phase.
- Stress-dependency correlations for model parameters could be incorporated into the hybrid model based on fittings of experimental results collected at various stress levels, which enabled prediction of the creep response under a given stress level using hybrid model.

Overall, this study provided insights into experimental tests and an interpretation thereof aiming at evaluating the creep behavior of grouted anchors embedded in clayey soils with varying moisture states. The time-dependent shear strength reduction of anchor–soil interface was investigated in relation to the moisture conditions of the surrounding clayey soils. The rheological hybrid model proposed in this study to characterize the anchor–soil interface shear creep response is expected to facilitate the understanding of long-term behavior of grouted anchors in clayey soils. Ultimately, the models and findings achieved in this study are expected to facilitate the decision-making process regarding the anticipated performance of grouted anchors in areas characterized by the presence of clayey soils, particularly those requiring long design life.

References

1. Acharya MP, Hendry MT, Martin CD (2018) Creep behavior of intact and remoulded fibrous peat. Acta Geotech 13(2):399–417

2. Becker LDB, Nunes ALLS (2015) Influence of soil confinement on the creep behavior of geotextiles. Geotext Geomembr 43(4):351–358

3. Benmokrane B, Ballivy G (1991) Five-year monitoring of load losses on prestressed cement-grouted rock anchors. Can Geotech J 28(5):668–677. https://doi.org/10.1139/t91-081

4. Benmokrane B, Chennouf A, Mitri HS (1995) Laboratory evaluation of cement-based grouts and grouted rock anchors. Int J Rock Mech Min Sci Geomech Abstr 32(7):633–642. https://doi.org/10.1016/0148-9062(95)00021-8

5. Borana L, Yin JH, Singh DN, Shukla SK, Pei HF (2017) Influences of initial water content and roughness on skin friction of piles using FBG technique. Int J Geomech 17(4):04016097. https://doi.org/10.1061/(asce)gm.1943-5622.0000794

6. Cao W, Yuan J, Wang J, Zhai Y (2013) A damage simulation technique of the full rock creep process considering accelerated creep. J Hunan Univ Nat Sci 40(2):15–20

7. Chen C, Liang G, Tang Y, Xu Y (2015) Anchoring solid–soil interface behavior using a novel laboratory testing technique. Chin J Geotech Eng 37(6):1115–1122

8. Chen S, Zhang X, Shahrour I (2015) Composite element model for the bonded anchorage head of stranded wire cable in tension. Int J Numer Anal Meth Geomech 39(12):1352–1368. https://doi.org/10.1002/nag.2364

9. Chen C, Liang G, Liu X, Tang Y, Xu Y, Liu J, Zhao Y, Li R (2016) A device and method for preparing soil samples used in testing frictional performance of anchor/pile-soil interface. China Patent ZL 2014 1 0176979.8, filed April 29, 2014, and issued July 6, 2016

10. Chen C, Liang G, Zhang G, Tang Y, Zheng X, Sun Y, Wang S, Wang C (2016) A testing system and method for frictional performance of anchor/pile-soil interface. China Patent ZL 2014 1 0176877.6, filed April 29, 2014, and issued March 30, 2016

11. Chen C, Zhang G, Zornberg JG, Zheng X (2018) Element nail pullout tests for prediction of soil nail pullout resistance in expansive clays. Geotech Test J. https://doi.org/10.1520/GTJ20170431

12. Chen W, Liu K, Feng W, Borana L, Yin J (2019) Influence of matric suction on nonlinear time dependent compression behavior of a granular fill material. Acta Geotech. https://doi.org/10.1007/s11440-018-00761-y

13. Cook RA, Douglas EP, Davis TM, Liu C (2013) Long-term performance of epoxy adhesive anchor systems. NCHRP Report 757, Transportation Research Board, Washington DC

14. Desai CS, Muqtadir A, Scheele F (1986) Interaction analysis of anchor–soil systems. J Geotech Eng 112(5):537–553. https://doi.org/10.1061/(ASCE)0733-9410(1986)112:5(537)

15. Deshmukh VB, Dewaikar DM, Choudhury D (2010) Computation of uplift capacity of pile anchors in cohesionless soil. Acta Geotech 5:87–94. https://doi.org/10.1007/s11440-010-0111-6

16. Ehrlich M, Silva RC (2015) Behavior of a 31 m high excavation supported by anchoring and nailing in residual soil of gneiss. Eng Geol 191:48–60. https://doi.org/10.1016/j.enggeo.2015.01.028

17. Gurinsky MA (2002) Long-term strength of prestressed ground anchors in creep-sensitive soils. American Society of Civil Engineers, International Deep Foundations Congress 2002—Orlando, Florida, United States (February 14–16, 2002), pp 37–52. https://doi.org/10.1061/40601(256)4

18. Hong CY, Yin JH, Zhou WH, Pei HF (2012) Analytical study on progressive pullout behavior of a soil nail. J Geotech Geoenviron Eng 138(4):500–507. https://doi.org/10.1061/(ASCE)GT.1943-5606.0000610

19. Hossain MA, Yin JH (2012) Influence of grouting pressure on the behavior of an unsaturated soil–cement interface. J Geotech Geoenviron Eng 138(2):193–202

20. Hossain MA, Yin JH (2014) Behavior of a pressure-grouted soil–cement interface in direct shear tests. Int J Geomech 14(1):101–109. https://doi.org/10.1061/(ASCE)GM.1943-5622.0000301

21. Hou XY, Li XF (1987) Time-effect of soil anchors in submerged soft ground. J Tongji Univ 15(2):147–156

22. JTG E40-2007, Test methods of soils for highway engineering, Ministry of Transportation of China, Beijing, China. https://www.codeofchina.com

23. Kim NK (2003) Performance of tension and compression anchors in weathered soil. J Geotech Geoenviron Eng 129(12):1138–1150. https://doi.org/10.1061/(asce)1090-0241(2003)129:12(1138)

24. Kim NK, Park JS, Kim SK (2007) Numerical simulation of ground anchors. Comput Geotech 34(6):498–507. https://doi.org/10.1016/j.compgeo.2006.09.002

25. Kränkel T, Lowke D, Gehlen C (2015) Prediction of the creep behavior of bonded anchors until failure—a rheological approach. Constr Build Mater 75:458–464. https://doi.org/10.1016/j.conbuildmat.2014.11.048

26. Li P, Liu J, Zhu JB, He HJ (2008) Research on effects of water content on shear creep behavior of weak structural plane of sandstone. Rock Soil Mech 29(7):1865–1871

27. Littlejohn S (2007) Ground anchorages and anchored structures in service. Thomas Telford, London

28. Liu L, Xu W (2015) Experimental researches on long-term strength of granite gneiss. Adv Mater Sci Eng 2:1–9. https://doi.org/10.1155/2015/187616

29. Liu J, Wang L, Pei J, Zheng L, Bian Y (2015) Experimental study on creep deformation and long-term strength of unloading-fractured marble. Eur J Environ Civ Eng 19(s1):97–107. https://doi.org/10.1080/19648189.2015.1064623

30. Liu Y, Liu C, Kang Y, Wang D, Ye D (2015) Experimental research on creep properties of limestone under fluid–solid coupling. Environ Earth Sci 73(11):7011–7018. https://doi.org/10.1007/s12665-015-4022-6

31. Liu X, Wang J, Huang J, Jiang H (2017) Full-scale pullout tests and analyses of ground anchors in rocks under ultimate load conditions. Eng Geol 228:1–10. https://doi.org/10.1016/j.enggeo.2017.07.004

32. Lu P, Zeng J, Sheng Q (2008) Creep tests on soft clay and its empirical models. Rock Soil Mech 29(4):1041–1052

33. Majda P, Skrodzewicz J (2009) A modified creep model of epoxy adhesive at ambient temperature. Int J Adhes Adhes 29(4):396–404. https://doi.org/10.1016/j.ijadhadh.2008.07.010

34. Martín LB, Tijani M, Hadj-Hassen F (2011) A new analytical solution to the mechanical behavior of fully grouted rockbolts subjected to pull-out tests. Constr Build Mater 25(2):749–755. https://doi.org/10.1016/j.conbuildmat.2010.07.011

35. McGown A, Andrawes KZ, Kabir MH (1982) Load-extension testing of geotextiles confined in soil. In: Proceedings of the second international conference on geotextiles, Las Vegas, USA, vol 3, pp 793–798

36. Menoudy AE, Soudki K (2014) Effects of various environmental exposures and sustainable load levels on the service life of

postinstalled adhesive anchors. J Mater Civ Eng 26(5):863–871. https://doi.org/10.1061/(ASCE)MT.1943-5533.0000878

37. Mesri G, Febres-Cordero E, Shields DR, Castro A (1981) Shear stress–strain–time behavior of clays. Geotechnique 31(4):537–552

38. National Transportation Safety Board (NTSB) (2007) Ceiling collapse in the interstate 90 connector tunnel Boston Massachusetts, July 10, 2006. Technical Report, Washington DC

39. Pei HF, Yin JH, Zhu HH, Hong CY (2013) Performance monitoring of a glass fiber-reinforced polymer bar soil nail during laboratory pullout test using FBG sensing technology. Int J Geomech 13(4):467–472. https://doi.org/10.1061/(asce)gm.1943-5622.0000226

40. Prieto-Muňoz PA, Yin HM, Testa RB (2013) Mechanics of an adhesive anchor system subjected to a pullout load. II: viscoelastic analysis. J Struct Eng 140(2):04013053. https://doi.org/10.1061/(ASCE)ST.1943-541X.0000822

41. Prisco C, Pisanò F (2014) Numerical modelling and mechanical analysis of an innovative soil anchoring system. Acta Geotech 9:1013–1028. https://doi.org/10.1007/s11440-013-0250-7

42. Puigvert F, Crocombe AD, Gil L (2014) Fatigue and creep analyses of adhesively bonded anchorages for CFRP tendons. Int J Adhes Adhes 54:143–154. https://doi.org/10.1016/j.ijadhadh.2014.05.013

43. Sabatini PJ, Pass DG, Bachus RC (1999) Geotechnical engineering circular no. 4—ground anchors and anchored systems. Federal Highway Administration, USA

44. She C (2009) Research on nonlinear viscoelasto-plastic creep model of rock. Chin J Rock Mechan Eng 28(10):2006–2011

45. Shen M, Chen H, Zhang Q (2012) Method for determining long-term strength of discontinuity using shear creep test. Chin J Rock Mechan Eng 31(1):1–7

46. Su LJ, Chan TCF, Shiu YK, Cheung T, Yin JH (2007) Influence of degree of saturation on soil nail pullout resistance in compacted completely decomposed granite fill. Can Geotech J 44(11):1314–1328. https://doi.org/10.1139/T07-056

47. Su LJ, Chan TCF, Yin JH, Shiu YK, Chiu SL (2008) Influence of overburden pressure on soil–nail pullout resistance in a compacted fill. J Geotech Geoenviron Eng 134(9):1339–1347. https://doi.org/10.1061/(ASCE)1090-0241(2008)134:9(1339)

48. Su LJ, Yin JH, Zhou WH (2010) Influences of overburden pressure and soil dilation on soil nail pull-out resistance. Comput Geotech 37(4):555–564. https://doi.org/10.1016/j.compgeo.2010.03.004

49. Sun J (1999) Rheological behavior of geomaterials and its engineering applications. China Architecture and Building Press, Beijing

50. Tan TK (1964) Determination of the rheological parameters hardening coefficients of clays. In: IUTAM symposium on rheology and soil mechanics, pp 266–273

51. Tan TK (1982) The mechanical problems for the long-term stability of underground galleries. Chin J Rock Mechan Eng 1(1):1–20

52. Tan TK, Kang WF (1980) Locked in stresses, creep and dilatancy of rocks, and constitutive equations. Rock Mech 13(1):5–22. https://doi.org/10.1007/BF01257895

53. Xanthakos PP (1991) Ground anchors and anchored structures. Wiley, Hoboken

54. Xu HF, Wang FJ, Cheng XX (2007) Pullout creep properties of grouted soil anchors. J Cent South Univ Technol 14(S1):474–477. https://doi.org/10.1007/s11771-007-0310-y

55. Yang M, Zhao Y, Zhang N (2014) Creep behavior of epoxy-bonded anchor system. Int J Rock Mech Min Sci 67:96–103. https://doi.org/10.1016/j.ijrmms.2014.02.001

56. Yeo SS, Hsuan YG (2010) Evaluation of creep behavior of high density polyethylene and polyethylene-terephthalate geogrids. Geotext Geomembr 28:409–421

57. Yin JH (2015) Fundamental issues of elastic viscoplastic modelling of the time-dependent stress–strain behavior of geomaterials. Int J Geomech 15(5):A4015002. https://doi.org/10.1061/(ASCE)GM.1943-5622.0000485

58. Yin JH, Zhou WH (2009) Influence of grouting pressure and overburden stress on the interface resistance of a soil nail. J Geotech Geoenviron Eng 135(9):1198–1208. https://doi.org/10.1061/(ASCE)GT.1943-5606.0000045

59. Zhao D, Hattab M, Yin ZY, Hicher PY (2018) Dilative behavior of kaolinite under drained creep condition. Acta Geotech. https://doi.org/10.1007/s11440-018-0686-x

60. Zornberg JG, Byler BR, Knudsen J (2004) Creep of geotextiles using time-temperature superposition methods. J Geotech Geoenviron Eng 130(11):1158–1168